Society of Medical Education & Research

2022, Volume 2, Issue 1, Page No: 130-147

ISSN: 3108-4834

Archive of International Journal of Cancer and Allied Science

Mast Cells Directly Engage with Colorectal Cancer Cells to Drive Epithelial-to-Mesenchymal Transition

Nikolaos Dimitris Papadopoulos[1]*, Giorgos Konstantinos Vlachos[1]

[1]Department of Oncology, National and Kapodistrian University of Athens, Athens, Greece.

***E-mail** ✉ n.papadopoulos.med@outlook.com

Abstract

Mast cells (MCs), a type of granulocytic immune cell, can either support or inhibit colorectal cancer (CRC) progression. This duality may result from subtype-specific interactions between MCs and CRC cells. Notably, BRAF-mutant CRCs are enriched in intestinal secretory cell populations. Our study reveals that MCs are particularly abundant in BRAF-mutant CRC, likely attracted by factors secreted by these tumor-associated secretory cells. Using direct coculture experiments, we found that MCs induce epithelial-to-mesenchymal transition (EMT) in CRC cells, requiring both physical contact and calcium signaling. Disrupting LFA-1/ICAM1 integrin binding attenuated EMT-associated marker expression triggered by coculture. Moreover, MCs can transfer biomolecules, including mRNA, to CRC cells during these interactions. This research highlights a previously unreported contact-dependent pro-tumor role of MCs in CRC and demonstrates intercellular molecular transfer, suggesting that targeting MC–CRC interactions, especially through integrin pathways, may offer novel therapeutic strategies for aggressive CRC variants.

Keywords: Mast cells, Cancer cells, Colorectal cancer, Epithelial-to-mesenchymal transition

Introduction

Colorectal cancer (CRC) is among the most frequently diagnosed cancers in the United States and ranks second in cancer-related mortality [1]. Roughly a quarter of patients initially diagnosed with primary CRC later develop metastases [2]. While early-stage disease can often be cured surgically, metastatic CRC is challenging to treat due to widespread dissemination of malignant cells. Despite recent advances that have improved survival, treatment efficacy is limited by tumor heterogeneity and the complexity of the immune microenvironment [2].

Access this article online https://smerpub.com/

Received: 27 February 2022; **Accepted:** 03 June 2022

How to cite this article: Papadopoulos ND, Vlachos GK. Mast Cells Directly Engage with Colorectal Cancer Cells to Drive Epithelial-to-Mesenchymal Transition. Arch Int J Cancer Allied Sci. 2022;2(1):130-47. https://doi.org/10.51847/EzeMjxHQnU

Patients with BRAF V600E mutations generally exhibit poor chemotherapy responses, and survival outcomes are worse than in other CRC subtypes [3, 4]. BRAF mutations often co-occur with microsatellite instability (MSI), which enhances infiltration of antitumor immune cells and improves responsiveness to immunotherapy [5]. However, approximately half of BRAF-mutant CRCs are microsatellite-stable (MSS), lacking significant immune infiltration and showing poor responses to immune checkpoint inhibitors [5]. Preclinical studies indicate that immune cell composition differs between BRAF-mutant and wild-type CRCs [6]. Understanding how the tumor immune microenvironment is modulated in MSS BRAF-mutant CRC is therefore essential for developing effective immunotherapies.

Recent work has shown that BRAF-mutant CRCs harbor increased populations of secretory cells, including enteroendocrine and goblet cells [7]. In the normal intestine, these cells recruit and interact with immune populations, such as MCs [8–12]. Accordingly, secretory

cells in BRAF-mutant CRC may shape tumor–immune interactions.

MCs, tissue-resident granulocytes, contribute to tumor progression by promoting angiogenesis, growth, and epithelial-to-mesenchymal transition (EMT), a key step in metastasis [13, 14]. However, their role in CRC is controversial: some studies report MC-mediated inhibition of tumor growth and induction of apoptosis [15, 16], while others show MCs enhancing growth and invasion without clear mechanistic insight [15]. These discrepancies may reflect subtype-specific differences. We therefore focused on BRAF-mutant CRC to explore potential unique interactions between secretory cells and MCs.

In this study, we demonstrate that MCs accumulate in human and murine BRAF-mutant CRC tumors, and that secretory cells promote MC migration in vitro. MCs induce EMT in CRC cells via contact- and calcium-dependent, integrin-mediated mechanisms, requiring AKT activation in both cell types. Additionally, MC-derived biomolecules are transferred into CRC cells. These findings provide novel insights into MC-driven EMT and describe previously unrecognized cellular interactions in CRC.

Materials and Methods

Cell lines and organoids

All cell cultures were maintained at 37°C with 5% CO_2. HT-29 and SW403 cells were cultured in McCoy's 5A and RPMI 1640 media (Corning) supplemented with 10% FBS. Both cell lines were obtained from ATCC and confirmed mycoplasma-free using a Universal Detection Kit (ATCC). The LAD2 human MC line (kindly provided by Dr. Dean Metcalfe, NIH/NIAID) was maintained in StemPro medium containing L-glutamine, antibiotics, and SCF [17, 18]. Human bone marrow $CD34^+$ cells (StemCell Technologies) were differentiated into bone marrow-derived MCs (BMMCs) using SCF, IL6, and IL3 for one week, with cells used after four weeks. BRAFV600E-mutant colon organoids were derived from patient-derived xenografts from the NCI PDMR and cultured as previously described [7, 19]. Cells used for experiments were under passage 15.

Coculture system and treatments

Cancer cells were plated 24 h prior to coculture. On the day of coculture, cells were washed with PBS and LAD2 MCs were added in a 1:1 ratio. Cocultures were maintained in SCF-free StemPro medium for defined durations. After incubation, the medium containing MCs was collected, centrifuged, and cell pellets retained for downstream applications. Cancer cells were washed thrice with PBS, scraped, and centrifuged, with pellets collected for analysis. LAD2 cells were passaged one day prior to each experiment. For migration studies, BMMCs and cancer cells were starved overnight in SCF- or FBS-free media. Treatments included Reparixin, Calcium Ionophore, BAPTA-AM, LY294002, Borussertib, BIRT-377, and Lifitegrast (MedChemExpress, Sigma-Aldrich), dissolved in DMSO. For LY294002, BIRT-377, and Lifitegrast, MCs were pretreated for 1 h before coculture, with drugs maintained throughout due to reversibility.

Immunohistochemistry (IHC)

Archived, deidentified human colorectal cancer tissues were obtained with approval from the Institutional Review Board, including five tumors harboring BRAF mutations and five non-BRAF–mutant adenocarcinomas matched for sex, age, and primary versus metastatic status [6]. Mouse tumor samples (Min and BLM models) were sourced from previously published work [6]. All procedures involving animals were conducted under protocols approved by the Indiana University Bloomington Animal Care and Use Committee, in line with AAALAC International standards. IHC staining and scoring were performed as detailed in the Supplementary Methods. Sample numbers were determined based on tissue availability rather than formal statistical power calculations.

Mouse mast cell analysis by flow cytometry (FACS)

Following tissue dissociation, single-cell suspensions were prepared and incubated with a fixable viability dye along with antibodies for surface and intracellular markers. Surface staining was conducted in FACS buffer using CD117 (c-Kit; Biolegend 105808) and CD129 (IL9R; Millipore/Sigma-Aldrich MABF2304F) for 30–60 minutes at 4°C. Cells were subsequently fixed in IC fixation buffer (Invitrogen) for 20 minutes at 4°C in the dark. For intracellular labeling, cells were washed in permeabilization buffer and stained sequentially for 5 and 60 minutes. Following three washes in FACS buffer, samples were run on an Attune flow cytometer and analyzed using FlowJo software.

Preparation of conditioned medium

To generate conditioned media, cancer cells expressing either empty vector (EV) or knockdown (KD) constructs were cultured to full confluency. Standard growth medium was replaced with serum-free medium for 48 hours. The supernatant was collected, centrifuged at 500×g for 5 minutes at 4°C, and used in migration assays.

Migration assays

For cancer cell migration, cells were plated onto the upper chambers of 8 µm PET transwell inserts (Corning, 3422) in 24-well plates. LAD2 cells were added at a 1:1 ratio 24 hours later and cocultured for 12 hours. After incubation, LAD2 cells were removed, and cancer cells were washed three times with PBS. The lower chamber was supplemented with 20% FBS and incubated for 24 hours before staining inserts with Hema 3 Stat Pack (Thermo Fisher Scientific, #123–869). Edge regions (outer 5% of the insert) were excluded during manual counting to minimize bias. Imaging was performed using an EVOS FL Auto microscope.

For MC migration, assays used 5 µm PET membrane transwells (Corning, 3421) in 24-well plates. Conditioned media from EV or KD cells served as chemoattractants, with unconditioned media as a control. BMMCs (5×10^4 cells/mL) were starved overnight, resuspended in the appropriate medium, and allowed to migrate overnight. Cells that migrated were lysed, and DNA quantified using the CyQUANT™ NF Cell Proliferation Assay. Fluorescence readings (480/520 nm) were used to calculate migration, with experiments performed in triplicate and repeated at least three times. A standard curve correlating relative fluorescence units (RFUs) to cell number was generated using known cell quantities according to the CytoSelect™ 24-Well Cell Migration Assay protocol (Cell BioLabs, Inc).

Organoid-based migration assays were performed with 817 BRAFV600E organoids embedded in 50% Matrigel (Corning, 356234). Five days post-seeding, LAD2 cells labeled with DiO (10 µg/mL, Invitrogen D275) were washed and added to organoid cultures. After 24 hours, unincorporated LAD2 cells were removed by washing with PBS. Imaging was conducted using an Olympus OSR spinning disk confocal system (IX83 inverted microscope) with CellSense software. LAD2 cells incorporated into the organoid-containing Matrigel were quantified across multiple biological replicates using z-stack imaging with 20 µm intervals.

Secreted factor profiling

Conditioned media from EV and ATOH1 KD cells (N = 3 per condition) were collected, centrifuged at 500×g for 5 minutes at 4°C, and analyzed for cytokines and chemokines using the Human Cytokine/Chemokine 96-Plex Discovery Assay® (HD96, Eve Technologies, Calgary, AB).

Immunofluorescence and confocal imaging

Cancer cells were plated on No. 1.5 coverslips for vimentin staining. Cells were labeled with Vybrant™ DiI (Invitrogen, V22885) and cocultured with LAD2 cells at a 1:1 ratio for 3 hours. Cells were then washed three times with PBS and stained with anti-vimentin antibody (CST #5741, 1:50). Confocal imaging was performed using a Leica STELLARIS 8 Falcon scanning system with MDi8 inverted microscope and LASX software at 63× magnification (1.2 A water immersion). Background signals were removed using ImageJ, and green fluorescence was quantified as integrated density (IntDen). A minimum of six images per condition were analyzed in independent replicates.

Live cell imaging

Cancer cells were seeded on Poly-D-lysine-coated glass-bottom dishes (Thermo Fisher, 150680). The following day, unlabeled or DiO-labeled (10 µg/mL, Invitrogen D275) LAD2 cells or BMMCs were added in HEPES Tyrode's buffer and immediately imaged. Imaging was performed on an Olympus OSR spinning disk confocal microscope with IX83 inverted system using 40× or 60× objectives (0.95 A water or 1.3 A silicon immersion, respectively) at 37°C and 5% CO_2. Images were processed in ImageJ.

RNA extraction and RT-qPCR

Total RNA was isolated from cell pellets using the RNeasy Mini Kit (Qiagen #74104) following manufacturer instructions. cDNA synthesis was performed using the Maxima First Strand cDNA Synthesis Kit (Thermo Fisher #K1642). RT-qPCR was conducted using gene-specific primers and FastStart Essential DNA Green Master (Roche #06402712001) [19]. Expression levels of target genes were normalized to RHOA. Primer sequences are listed in the Supplementary Methods.

Knockdown and plasmid constructs

Details of shRNA constructs and plasmids are provided in the Supplementary Methods. Lentiviral production was carried out as previously described [19].

Mast cell spinoculation

Mast cells (5×10^5) were gently resuspended in 200 µL of fresh SP34 medium, combined with 50 µL of Vimentin-Flag (Vim-Flag) viral particles supplemented with 8 µg/mL polybrene, and plated in 12-well culture plates. The cell-virus mixture was centrifuged at 1500×g for 90 minutes at 30°C to facilitate viral entry. Following spinoculation, fresh culture medium was added, and the cells were returned to standard growth conditions. The subsequent day, cells were resuspended in fresh medium and immediately applied in downstream experimental assays.

Statistical analyses

All quantitative PCR and functional assay results were analyzed using GraphPad Prism 10. Variances across groups were assessed and found to be comparable. The exact statistical methods for each experiment are specified in the figure legends. Typically, experiments were conducted with three independent biological replicates and repeated multiple times, often three iterations per assay. Sample sizes were determined from preliminary studies to ensure sufficient power to detect meaningful differences. All samples were included in the analysis. qRT-PCR experiments using HT-29 cells cocultured with LAD2 cells were performed N = 3 independent times with three biological replicates per experiment. For SW403 cells cocultured with LAD2 cells, and HT-29 cells cocultured with BMMCs, qRT-PCR was conducted N = 1 or N = 2 independent times with three biological replicates each. Western blot images shown are representative, with replicate numbers indicated in figure legends; all bands for a given experiment were derived from the same membrane unless specified otherwise.

Results and Discussion

Preferential accumulation of mast cells in BRAF-mutant colorectal cancer

BRAF-mutant and BRAF-wild-type colorectal tumors display marked differences in cellular composition and immune profiles. To explore potential disparities in immune infiltration, we examined mast cell presence in these tumor subtypes. Prior work comparing the tumor immune landscape in BRAF-mutant (Braf^V600E Lgr5^Cre Min; BLM) versus BRAF-wild-type (Min) mouse colon tumors demonstrated via CIBERSORT analysis of RNA-sequencing data that mast cells are more abundant in BRAF-mutant tumors [6]. In addition, BLM tumors exhibited higher expression of mast cell-specific proteases compared to Min tumors **(Figure 1a)**. IHC staining confirmed increased numbers of MCPT1-positive mast cells in BLM tumors **(Figures 1b and 1c)**. Flow cytometry further supported these findings, revealing greater frequencies of $IL9^+$ $c\text{-}Kit^+$ mast cells in BLM tumors relative to Min tumors and normal colonic epithelium **(Figure 1d)**.

To validate these observations in human colorectal cancer, we analyzed The Cancer Genome Atlas (TCGA) colon adenocarcinoma (COAD) dataset [20, 21] using CIBERSORT. Results indicated a trend toward higher activated mast cell populations in BRAF-mutant tumors compared to BRAF-wild-type ($p = 0.0660$, **(Figure 1e)**). Complementary IHC analysis of human tissue revealed an elevated number of tryptase-positive mast cells in BRAF-mutant tumors compared with BRAF-wild-type counterparts **(Figures 1f and 1g)**. Collectively, these findings indicate that mast cells are selectively enriched in BRAF-mutant colorectal cancers, suggesting a subtype-specific interaction between mast cells and tumor cells.

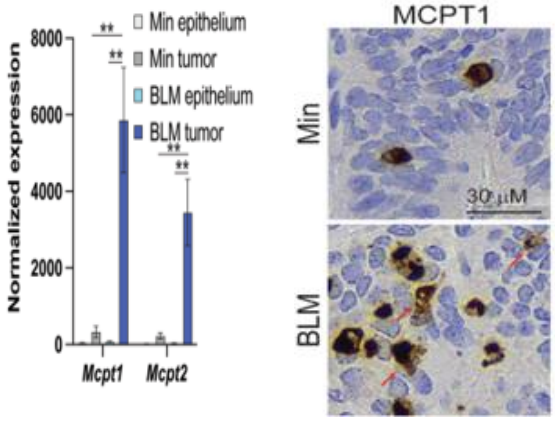

a) b)

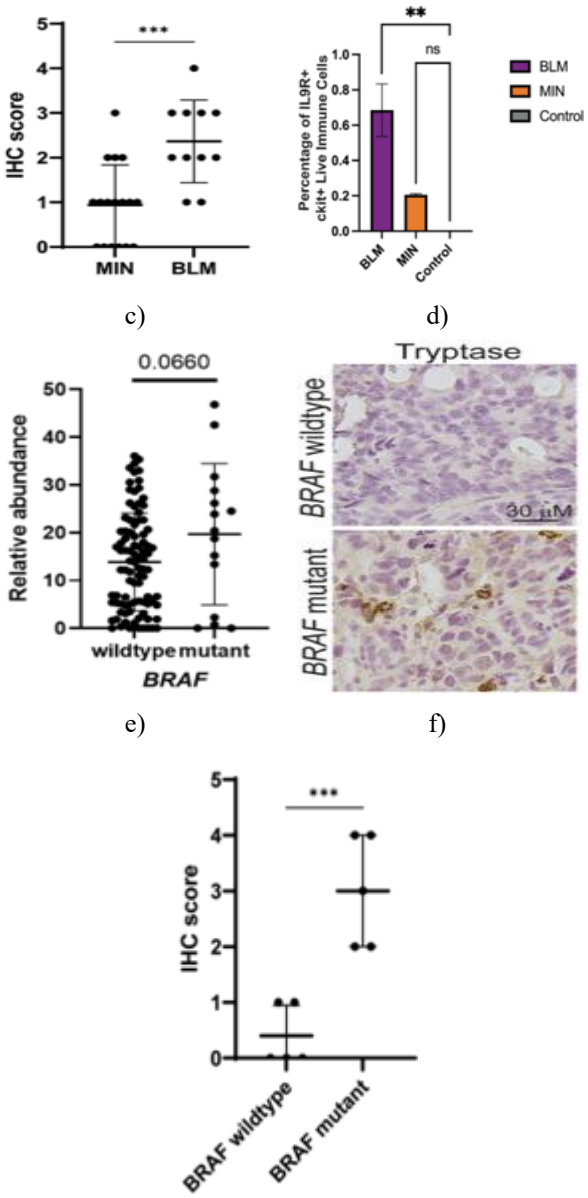

Figure 1. Increased presence of mast cells in colorectal cancers harboring BRAF mutations relative to those with wild-type BRAF. Panel a displays normalized gene expression levels from RNA-sequencing data for MCPT1 and MCPT2 in colonic epithelium from Min and BLM mice (N = 4) as well as in colonic tumors (N = 4–5). Panel B shows immunohistochemical staining for MCPT1 in tumors from Min and BLM mice, with red arrows highlighting degranulating mast cells. Panel c provides quantification of MCPT1-positive cells based on panel b, where each point corresponds to a single tumor, and bars denote mean values with standard deviation. Panel d indicates the proportion of immune cells expressing IL9R and c-KIT in BLM tumors, Min tumors, and healthy colonic epithelium (as control). Panel e depicts the relative levels of activated mast cells in human BRAF-mutant versus wild-type colorectal cancers, as assessed via CIBERSORT deconvolution of RNA-sequencing data from the TCGA COAD dataset, with each point representing one patient sample and bars showing mean ± SD. Panel f presents immunohistochemical staining for tryptase in human primary colorectal cancer tissues. Panel g quantifies tryptase-positive cells from panel F, plotted similarly to panel C. Across all panels, data are presented as mean ± SD, and statistical comparisons were performed using two-tailed Student's t-tests (*$p \leq 0.05$; **$p \leq 0.01$; ***$p \leq 0.001$; ****$p \leq 0.0001$; ns, not significant).

Secretory lineage cells in colorectal cancer attract mast cells through IL-8 secretion. Certain secretory lineages, such as enteroendocrine and goblet cells, which are particularly abundant in BRAF-mutant colorectal cancers [7], are known to engage with mast cells in the healthy intestine [8–12]. This raises the possibility that secretory components within colorectal tumors could modulate mast cell infiltration. To explore this, CD34+ progenitor cells from hematopoietic sources were differentiated into bone marrow-derived mast cells (BMMCs). Secretory lineages were then reduced in the BRAF-mutant colorectal cancer cell line HT-29 via shRNA targeting ATOH1 [7], a key transcription factor driving secretory progenitor specification from colonic stem cells [22] **(Figure 2a)**. Conditioned medium from ATOH1-depleted (KD) HT-29 cells, compared to control (empty vector, EV) cells, markedly decreased BMMC chemotaxis **(Figure 2b)**. NEUROG3 and GFI1 direct the specification of enteroendocrine and goblet lineages, respectively [23] **(Figure 2a)**. Reducing enteroendocrine cells through NEUROG3 knockdown had no notable impact on BMMC chemotaxis **(Figure 2c)**. In contrast, depleting goblet cells via GFI1 knockdown substantially impaired BMMC movement toward the conditioned medium **(Figure 2d)**.

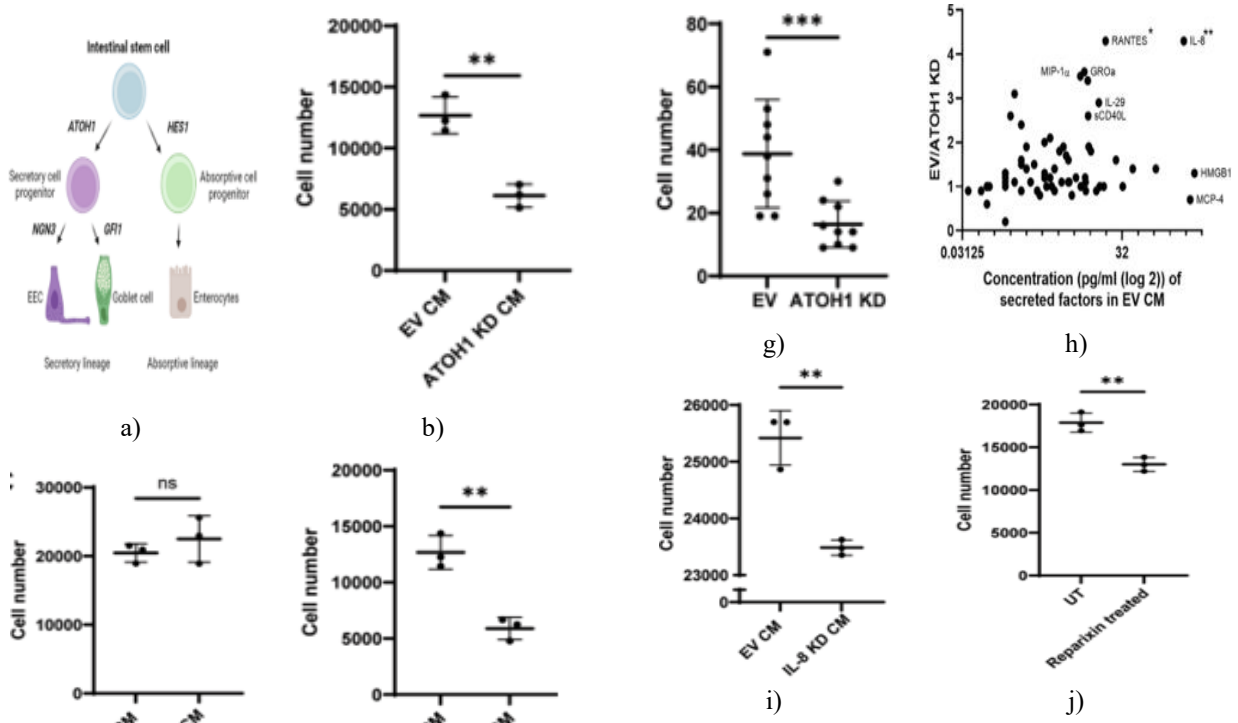

Figure 2. Secretory lineage cells in colorectal cancer attract mast cells to tumor-conditioned media primarily through the secretion of IL-8. Panel a depicts the differentiation hierarchy of normal colonic epithelium, showing how stem cells commit to either secretory or absorptive lineages, with key transcription factors indicated for each branch. EEC denotes enteroendocrine cells. Panel b quantifies the chemotaxis of bone marrow-derived mast cells (BMMCs) toward conditioned media (CM) from HT-29 cells transduced with empty vector (EV) or ATOH1 knockdown (KD), measured by DNA content in the lower transwell chamber and converted to cell counts using a standard curve. Data are shown as mean ± SD, with each point representing an independent biological replicate. Panel C shows BMMC migration toward CM from EV or GFI1 KD HT-29 cells, formatted as in panel b. Panel d presents BMMC migration toward CM from EV or NGN3 KD HT-29 cells, formatted as in panel B. Panels E and F display representative images from different focal planes in a z-stack of Matrigel domes containing EV (e) or ATOH1 KD (f) human CRC organoids (line 817), with migrated LAD2 mast cells labeled using DiO (10 µg/ml for 20 min, green fluorescence) after 24 hours of exposure in surrounding media. Scale bar represents 100 µm; magnification 10×. Red arrowheads point to LAD2 cells that have infiltrated

the Matrigel dome. Panel g quantifies migrated LAD2 cells from panels e and f, based on counts from three independent fields of view per condition (z-stacks). Panel h highlights differences in secreted factors (pg/ml) between EV and ATOH1 KD HT-29 cells, with EV/ATOH1 KD ratios shown; asterisks beside cytokine names denote statistical significance. Panel I assesses BMMC migration toward CM from EV or IL-8 KD HT-29 cells, formatted as in panel B. Panel J evaluates migration of untreated (UT) or Reparixin-treated (10 μM overnight) BMMCs toward HT-29 CM, formatted as in panel B. For all panels, N = 3; data are presented as mean ± SD, and statistical significance was assessed by two-tailed t-test (*p ≤ 0.05; **p ≤ 0.01; ***p ≤ 0.001; ****p ≤ 0.0001; ns, not significant).

To validate these observations in another system, secretory lineages were reduced in patient-derived BRAFV600E-mutant CRC organoids (817) via shRNA-mediated ATOH1 depletion. This resulted in markedly impaired migration of LAD2 cells toward ATOH1 KD organoid domes relative to EV controls **(Figures 2e–2g)**. Given that cytokines like SCF are established recruiters of mast cells during inflammation and that secretory components are prominent in BRAF-mutant CRC, potentially shaping the tumor secretome [15, 24], a cytokine profiling was conducted. IL-8 emerged as the most abundant cytokine in EV HT-29 conditioned media and the one most strongly reduced upon ATOH1 knockdown **(Figure 2h)**. To interrogate IL-8's contribution to BMMC recruitment, IL-8 (CXCL8) expression was first suppressed in HT-29 cells via knockdown. Despite only partial reduction in IL-8 levels, BMMC chemotaxis toward IL-8 KD conditioned media showed a clear downward trend compared to EV controls **(Figure 2i)**. Furthermore, pretreatment of BMMCs with Reparixin to block the IL-8 receptors CXCR1 and CXCR2 significantly diminished their migration toward HT-29 conditioned media relative to untreated cells **(Figure 2j)**. Collectively, these data indicate that IL-8 secreted by CRC secretory lineages plays a key role in mast cell attraction in vitro.

Mast cells drive epithelial-to-mesenchymal transition in colorectal cancer cells.

To investigate the pro-tumorigenic effects of mast cells in CRC, HT-29 cells were directly cocultured with the human mast cell line LAD2, which expresses FcεRI and characteristic proteases [17]. Post-coculture separation efficiency was confirmed by flow cytometry after labeling with CD45-AF488 (immune marker) and EPCAM-AF647 (epithelial marker), achieving >99% purity for LAD2 fractions and >98% for HT-29 fractions. Notably, coculture with LAD2 cells upregulated both mRNA and protein levels of EMT-associated genes SNAI2 (SNAI2), Vimentin (VIM), and ZEB2 (ZEB2) in HT-29 cells **(Figures 3a and 3b)**. CCL2 cytokine expression, included as an internal positive control, was also elevated in cocultured HT-29 cells and monitored throughout subsequent experiments. Comparable increases in VIM, CCL2, and ZEB2 were seen when HT-29 cells were cocultured with BMMCs. SW403, a BRAF wild-type mucinous CRC line harboring secretory cells [19], exhibited similar upward trends in EMT marker expression upon LAD2 coculture. Elevated Vimentin protein in cocultured HT-29 cells was additionally verified by immunofluorescence staining **(Figures 3c and 3d)**. As EMT induction is frequently linked to enhanced cell motility [25], prior exposure to LAD2 cells significantly boosted the migratory capacity of HT-29 cells in transwell assays compared to non-cocultured controls **(Figures 3e and 3f)**. These results collectively support a role for mast cells in facilitating epithelial-to-mesenchymal transition in colorectal cancer cells.

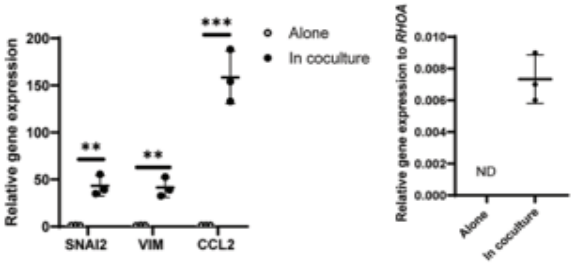

a)

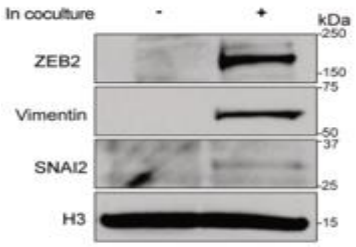

b)

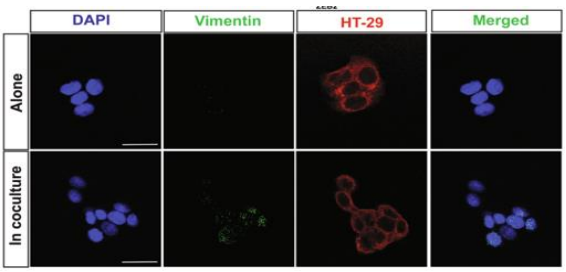

c)

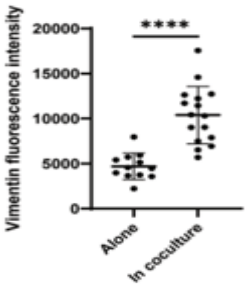

d)

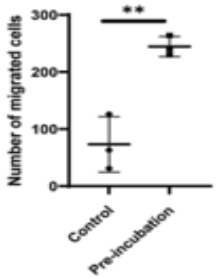

f)

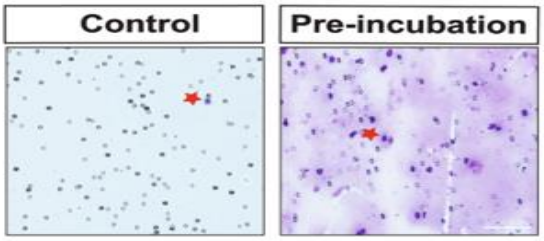

e)

Figure 3. Mast cells trigger the upregulation of epithelial-to-mesenchymal transition (EMT)-associated factors and enhance migratory behavior in colorectal cancer cells. Panel a presents relative mRNA levels of EMT-associated genes along with CCL2 (left panel) and ZEB2 (right panel, marked as not detected, ND) in HT-29 cells grown either alone or in direct coculture with LAD2 cells for 6 hours. Panel b displays a representative Western blot of HT-29 cells cultured alone or with LAD2 cells for 3 hours, from N = 3 independent experiments. Panel c provides representative immunofluorescence images showing Vimentin staining (green) in HT-29 cells (pre-labeled red with DiL, 10 µg/ml for 20 minutes) either alone or following 3-hour direct coculture with LAD2 cells. Scale bar represents 20 µm. Panel d quantifies Vimentin fluorescence intensity across at least six representative fields, with N = 2. Panel e shows images of transwell membranes with migrated HT-29 cells (highlighted by red stars) after prior incubation either alone (control) or with LAD2 cells for 12 hours, followed by a 24-hour migration period. Scale bar represents 100 µm. Panel f reports the total count of migrated HT-29 cells, with N = 3. In all panels, data are displayed as mean ± SD, and statistical comparisons were made using two-tailed t-tests (*p ≤ 0.05; **p ≤ 0.01; ***p ≤ 0.001; ****p ≤ 0.0001; ns, not significant).

Mast cells actively contribute to driving the EMT program in colorectal cancer cells

Calcium signaling is critical for mediator release, intracellular transduction, and overall activation in mast cells [26, 27]. Treatment of LAD2 cells with the intracellular calcium chelator BAPTA-AM effectively suppressed mediator secretion. In line with earlier observations, direct coculture between HT-29 and LAD2 cells elevated both gene and protein levels of EMT markers. However, pretreatment of LAD2 cells with BAPTA-AM prevented this upregulation of EMT-associated markers in the cocultured HT-29 cells **(Figures 4a and 4b)**. Comparable effects were noted when BAPTA-AM-pretreated bone marrow-derived mast cells (BMMCs) were cocultured with HT-29 cells, as well as when SW403 cells were exposed to BAPTA-AM-pretreated LAD2 cells. Pretreatment of LAD2 cells with BAPTA-AM did not alter Vimentin expression within the LAD2 population itself, providing additional evidence against cross-contamination into the cancer cell fraction. No notable changes in EMT-related gene expression were detected when HT-29 cells were pretreated with BAPTA-AM prior to coculture compared to untreated cocultured controls, indicating that calcium signaling within the cancer cells themselves is not required for the observed EMT marker induction.

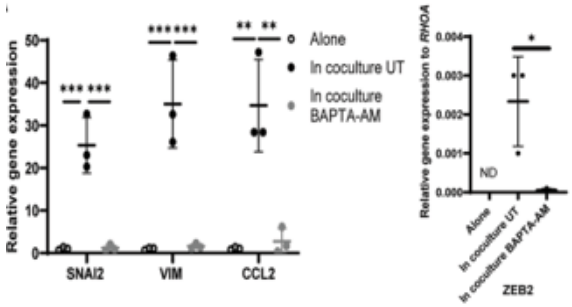

a)

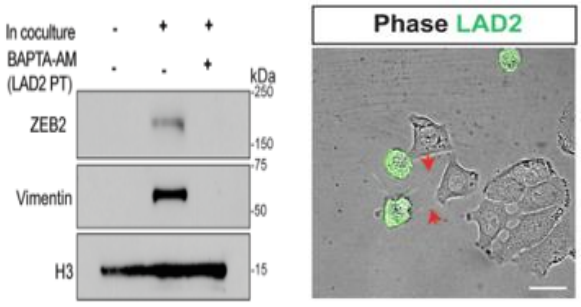

b)

c)

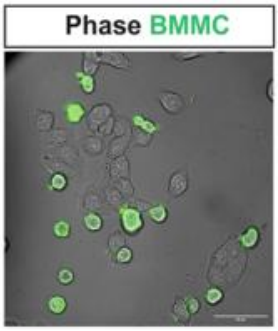

d)

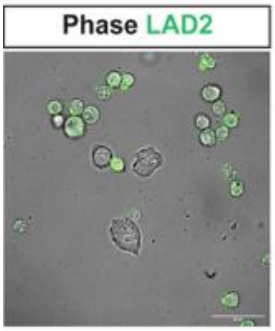

e)

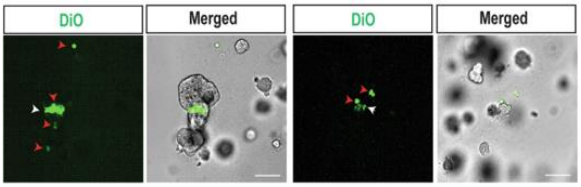

f)

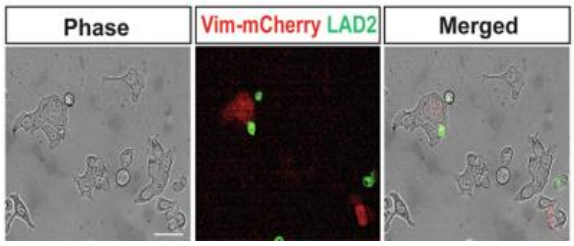

g)

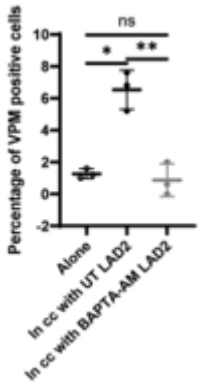

h)

Figure 4. Mast cells trigger epithelial-to-mesenchymal transition (EMT) in colorectal cancer cells through mechanisms requiring both calcium signaling and direct cell contact. Panel a shows relative qRT-PCR data for EMT-associated genes and CCL2 (left) as well as ZEB2 (right, labeled not detected, ND) in HT-29 cells cultured alone, in direct coculture with untreated (UT) LAD2 cells, or in coculture with LAD2 cells pretreated with BAPTA-AM (20 µM for 1 hour) for 6 hours. Panel b presents Western blots of HT-29 cells alone, cocultured with untreated LAD2 cells, or cocultured with BAPTA-AM-pretreated LAD2 cells (denoted LAD2 PT) for 3 hours, with N = 3. Panel c depicts live imaging of DiO-labeled LAD2 cells (10 µg/ml for 20 min, green) in direct coculture with unlabeled HT-29 cells, captured using an Olympus OSR SD confocal microscope over 4 hours; arrowheads highlight cytoplasmic extensions, at 100× magnification with a 20 µm scale bar. Panel d shows direct coculture of BMMCs with HT-29 cells, labeled and imaged similarly to panel C for 1 hour at 60× magnification. Panel e displays direct coculture of LAD2 cells with SW403 cells, labeled and imaged as in panel C for 1 hour at 60× magnification. Panel f provides representative images of DiO-labeled LAD2 cells (green, red arrowheads) in direct contact with 817 organoids, revealing green staining transfer (white arrowheads), at 10× magnification with a 100 µm scale bar. Panel g features HT-29 cells transfected with a Vimentin promoter-mCherry reporter plasmid cocultured with DiO-labeled LAD2 cells (green), imaged as in panel c for 4 hours at 40× magnification with a 50 µm scale bar. Panel h quantifies the percentage of mCherry-positive HT-29 cells when

cultured alone, in coculture with untreated (UT) LAD2 cells, or with BAPTA-AM-pretreated LAD2 cells; VPM indicates Vimentin promoter driving mCherry. Across panels, data are shown as mean ± SD, with points representing independent biological replicates; statistical tests include two-tailed t-test (A, right) and one-way ANOVA (A left, H) (*p ≤ 0.05; **p ≤ 0.01; ***p ≤ 0.001; ****p ≤ 0.0001; ns, not significant).

Mast cells typically exert effects through secretion of soluble mediators [28–32]. However, exposing HT-29 cells to either standard or concentrated conditioned media from cocultures yielded no notable changes in EMT marker gene expression relative to HT-29 cells alone, indicating that released soluble factors from mast cells are insufficient to drive EMT.

Live-cell imaging of LAD2-HT-29 cocultures uncovered physical interactions, including direct cell-cell contacts and cytoplasmic protrusions extending from LAD2 cells **(Figure 4c)**. Comparable patterns emerged in BMMC-HT-29 cocultures and LAD2-SW403 cocultures **(Figures 4d and 4e)**. Furthermore, 817 organoids physically contacting LAD2 cells exhibited green fluorescence, presumably from transfer of the lipophilic DiO dye used for LAD2 labeling **(Figure 4f)**. This prompted the hypothesis that EMT marker upregulation occurs specifically in HT-29 cells engaged in direct contact with mast cells, thereby activating the EMT program. To examine this, HT-29 cells expressing mCherry under the VIM promoter were cocultured with green-labeled LAD2 cells; clusters of mCherry-positive HT-29 cells were observed in direct contact or immediate proximity to LAD2 cells **(Figure 4g)**. Roughly 7 percent of HT-29 cells expressed mCherry upon LAD2 coculture versus ~1% when alone **(Figure 4h)**. In three independent experiments, 43 percent, 42 percent, and 14 percent of mCherry-positive HT-29 cells were in direct physical contact with mast cells. Coculture with BAPTA-AM-pretreated LAD2 cells reduced mCherry-positive HT-29 cells to levels similar to those cultured alone **(Figure 4h)**. These results collectively indicate that mast cells actively promote EMT marker expression in colorectal cancer cells via a contact-dependent process.

Inhibition of the PI3K/AKT pathway attenuates EMT marker upregulation in cocultured colorectal cancer cells

Pretreatment of LAD2 cells with BAPTA-AM altered their morphology yet did not abolish physical interactions with HT-29 cells. Notably, BAPTA-AM reduced AKT phosphorylation in LAD2 cells compared to controls, suggesting that AKT signaling may underpin mast cell-mediated EMT induction in cancer cells.

Treatment of direct cocultures with LY294002 (a reversible PI3K inhibitor) suppressed both mRNA and protein levels of most EMT markers in HT-29 cells relative to untreated cocultures **(Figures 5a and 5b)**. As anticipated, LY294002 diminished AKT activation in these cocultured HT-29 cells **(Figure 5b)**. Similar attenuation of coculture-induced EMT markers occurred in HT-29 cells exposed to BMMCs under LY294002 treatment **(Figures 5c and 5d)**. Likewise, LY294002 reduced EMT marker expression in SW403 cells cocultured with LAD2 cells.

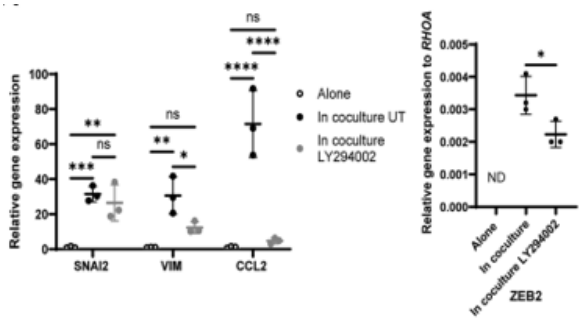

a)

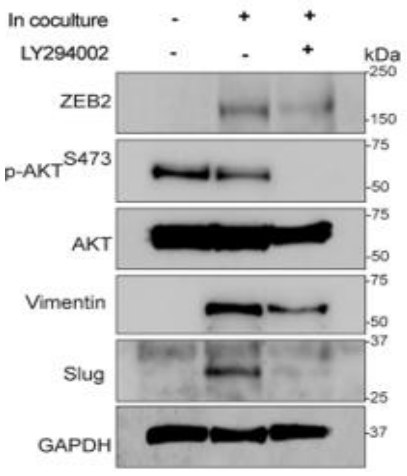

b)

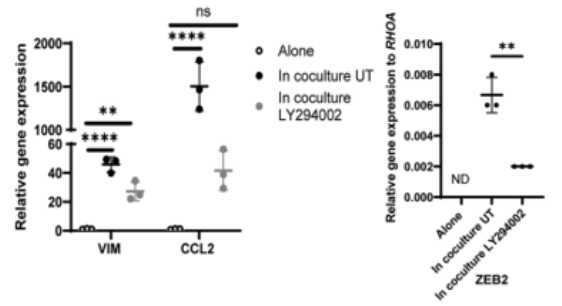

c)

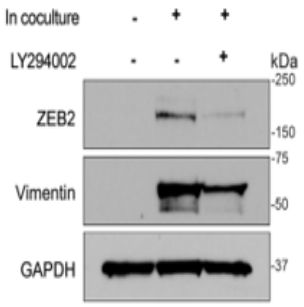

d)

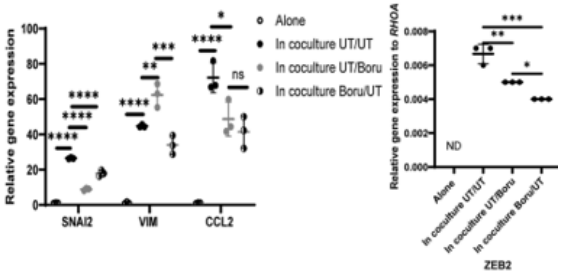

e)

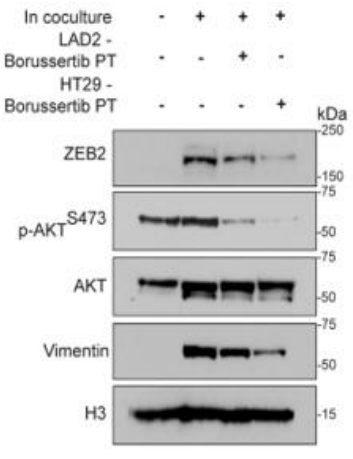

f)

Figure 5. AKT signaling contributes to the coculture-mediated upregulation of epithelial-to-mesenchymal transition (EMT)-associated markers in colorectal cancer cells. Panel a displays relative qRT-PCR results for EMT-related genes and CCL2 (left) as well as ZEB2 (right, marked not detected, ND) in HT-29 cells cultured alone, in direct coculture with untreated (UT) LAD2 cells, or in coculture with LAD2 cells exposed to LY294002 (50 µM). Panel b shows Western blots of HT-29 cells under the same conditions as panel a, with N = 3. Panel C presents relative qRT-PCR data for EMT-related genes and CCL2 (left) and ZEB2 (right, ND) in HT-29 cells alone, cocultured with untreated (UT) bone marrow-derived mast cells (BMMCs), or cocultured with BMMCs treated with LY294002 (60 µM). Panel d provides Western blots of HT-29 cells under the conditions described in panel c for 3 hours, with N = 1. Panel e reports relative qRT-PCR for EMT-related genes and CCL2 (left) and ZEB2 (right, ND) in HT-29 cells alone, untreated and cocultured with untreated LAD2 cells (UT/UT), untreated and cocultured with Borussertib-pretreated (1 µM overnight) LAD2 cells (UT/Boru), or Borussertib-pretreated (10 µM overnight) and cocultured with untreated LAD2 cells (Boru/UT) for 6 hours. Panel f shows Western blots of HT-29 cells under the conditions in panel e for 3 hours; HT-29 – Borussertib PT denotes pretreated HT-29 cells, and LAD2 – Borussertib PT denotes pretreated LAD2 cells, with N = 3. In all panels, data are presented as mean ± SD, with points indicating independent biological replicates; statistical analyses used two-tailed t-tests (a right, c right) and one-way ANOVA (a left, c left, E) (*$p \leq 0.05$; **$p \leq 0.01$; ***$p \leq 0.001$; ****$p \leq 0.0001$; ns, not significant).

To identify the cell type in which PI3K/AKT signaling is essential for EMT marker induction, LAD2 and HT-29 cells were separately pretreated with the irreversible AKT inhibitor Borussertib. Pretreatment of LAD2 cells alone with Borussertib attenuated the coculture-driven rise in mRNA and protein levels of most EMT markers in HT-29 cells, with the exception of VIM mRNA. However, Borussertib pretreatment of HT-29 cells yielded variable effects on ZEB2 and Vimentin protein across replicates **(Figures 5e and 5f)**. As anticipated, Borussertib reduced AKT phosphorylation in pretreated HT-29 cells, but pretreatment of LAD2 cells also diminished AKT activation in the partnering untreated HT-29 cells **(Figure 5f)**. Conversely, Borussertib exposure of HT-29 cells lowered activated AKT in untreated LAD2 cells. Separate Borussertib pretreatment

of either LAD2 or SW403 cells similarly suppressed coculture-induced EMT marker mRNA upregulation in SW403 cells, sparing ZEB2 mRNA. At the protein level in SW403 cells, ZEB2 and Vimentin induction persisted when LAD2 cells were pretreated but was abolished upon SW403 pretreatment. Unlike the outcomes with LAD2 cells under LY294002 or BMMC cocultures, individual Borussertib pretreatment of HT-29 cells or BMMCs failed to block coculture-mediated EMT marker upregulation in HT-29 cells despite reduced AKT phosphorylation in the cancer cells. Notably, basal AKT activation was minimally detectable in BMMCs compared to LAD2 cells.

LFA-1/ICAM-1 integrin interactions contribute to EMT marker induction in cocultured colorectal cancer cells.

Engagement of lymphocyte function-associated antigen 1 (LFA-1) and intercellular adhesion molecule-1 (ICAM-1) integrins has been implicated in natural killer cell immunological synapse formation with tumor targets [33]. Gene ontology analysis of RNA-sequencing data revealed significant enrichment of the "integrin binding" pathway in LAD2 cells following coculture with HT-29 cells relative to LAD2 cells alone. Additionally, ICAM-1 expression increased in cocultured HT-29 cells. Administration of the LFA-1 inhibitor BIRT-377 reduced both mRNA and protein levels of EMT markers in HT-29 cells cocultured with LAD2 cells compared to untreated cocultures **(Figures 6a and 6b)**. Comparable suppression occurred in HT-29 cells cocultured with BMMCs **(Figures 6c and 6d)**. BIRT-377 also diminished coculture-driven EMT marker upregulation in SW403 cells exposed to LAD2 cells. Furthermore, BIRT-377 exposure lowered the enhanced migration of HT-29 cells previously incubated with untreated LAD2 cells **(Figure 6e)**.

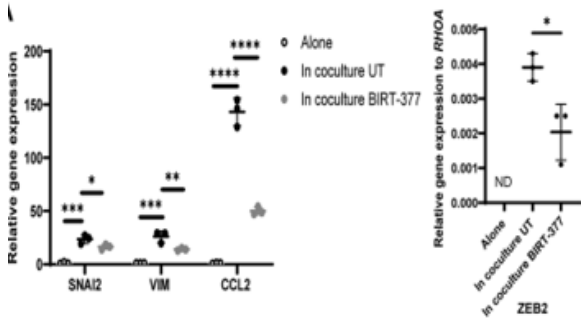

a)

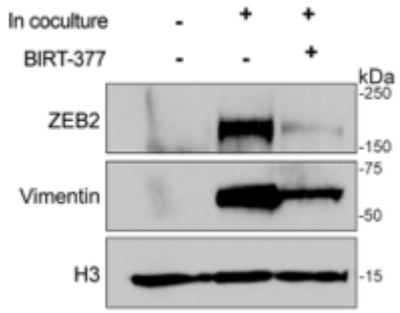

b)

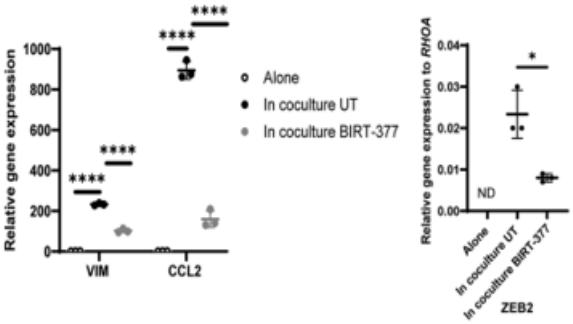

c)

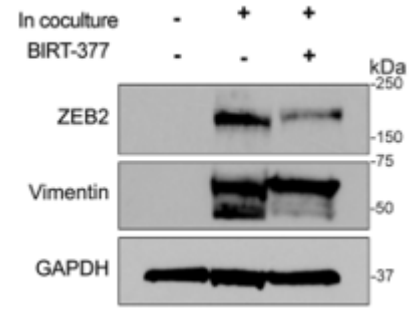

d)

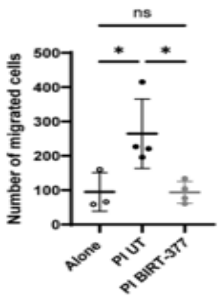

e)

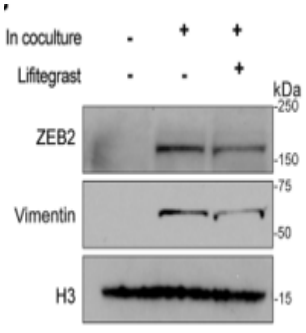

g)

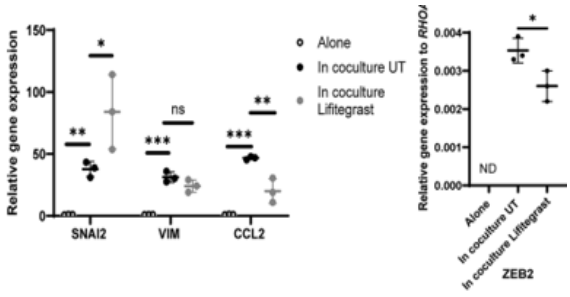

f)

Figure 6. Disrupting LFA-1/ICAM-1-mediated adhesion markedly attenuates the mast cell-driven upregulation of epithelial-to-mesenchymal transition markers in colorectal cancer cells grown in coculture. Panel a reports qRT-PCR quantification of EMT-associated transcripts together with CCL2 (left) and ZEB2 (right; labeled not detected, ND) in HT-29 cells maintained alone, cocultured with untreated LAD2 cells (UT), or cocultured with LAD2 cells in the presence of the LFA-1 antagonist BIRT-377 (20 µM) for 6 hours. Panel b shows immunoblot analysis of HT-29 cells under identical conditions for 3 hours (N = 3). Panel c presents qRT-PCR data for the same markers in HT-29 cells alone, cocultured with untreated bone marrow-derived mast cells (UT BMMCs), or cocultured with BMMCs exposed to BIRT-377 (40 µM) for 6 hours. Panel d displays corresponding immunoblots for 3-hour cocultures (N = 2). Panel e summarizes transwell migration results for HT-29 cells that were pre-exposed for 12 hours either alone, with untreated LAD2 cells (PI UT), or with BIRT-377-treated LAD2 cells (PI BIRT-377, 20 µM), followed by a 24-hour migration period (N = 3). Panel f shows qRT-PCR quantification of EMT markers and CCL2 (left) and ZEB2 (right, ND) in HT-29 cells alone, cocultured with untreated LAD2 cells, or cocultured with LAD2 cells treated with the alternative LFA-1 blocker Lifitegrast (40 µM) for 6 hours. Panel g provides immunoblots for the conditions described in panel F at 3 hours (N = 2). Data across panels are expressed as mean ± SD, with individual points denoting biological replicates. Statistical evaluation employed two-tailed t-tests (panel f right) or one-way ANOVA (panels a, c, e, f left); significance levels: *p ≤ 0.05, **p ≤ 0.01, ***p ≤ 0.001, ****p ≤ 0.0001, ns = not significant.

Treatment of LAD2–HT-29 cocultures with Lifitegrast yielded effects comparable to BIRT-377, reducing the coculture-associated elevation of most EMT markers in HT-29 cells, although SNAI2 transcript levels were largely unaffected **(Figures 6f and 6g)**. Parallel outcomes were obtained when HT-29 cells were cocultured with BMMCs under Lifitegrast.

Mast cells directly deliver Vimentin protein and mRNA to colorectal cancer cells

Direct cell-to-cell transfer of cellular components—including proteins, mRNA, vesicles, and organelles—has been widely documented [34–37]. To investigate whether mast cells could deliver Vimentin to adjacent tumor cells, LAD2 cells were engineered to express a FLAG-tagged Vimentin construct (Vim-Flag) and placed in direct coculture with HT-29 cells. Coculture with either empty-vector or Vim-Flag LAD2 cells raised endogenous Vimentin and ZEB2 protein in HT-29 cells, as previously observed. Strikingly, FLAG immunoreactivity was evident in HT-29 lysates only after exposure to Vim-Flag-expressing LAD2 cells, confirming intercellular transfer of the tagged protein **(Figure 7a)**. Pretreatment of Vim-Flag LAD2 cells with the calcium chelator BAPTA-AM abolished detectable Vim-Flag in partner HT-29 cells despite preserved expression in the mast cells themselves **(Figure 7a)**. Analogous transfer of Vim-Flag to SW403 cells was also prevented by BAPTA-AM pretreatment of LAD2 cells **(Figure 7b)**. BIRT-377 again suppressed overall EMT marker induction in HT-29 cocultures **(Figure 7c)** and concurrently reduced Vim-Flag delivery to HT-29 cells relative to vehicle-treated cocultures, without diminishing Vim-Flag levels in the mast cell population **(Figure 7c)**. Similar inhibition of transfer was noted in SW403 cells. Exposure of cocultures to the PI3K inhibitor LY294002 likewise impaired Vim-Flag translocation to HT-29 cells while leaving mast cell expression intact **(Figure 7D)**. Finally, Vim-Flag transcripts were detectable in HT-29 cells exclusively following coculture with Vim-Flag LAD2 cells **(Figure 7e)**. Taken together, these experiments demonstrate that mast cells shuttle both Vimentin protein and its encoding mRNA to colorectal cancer cells through a mechanism reliant on cell-contact integrin interactions and mast cell calcium signaling.

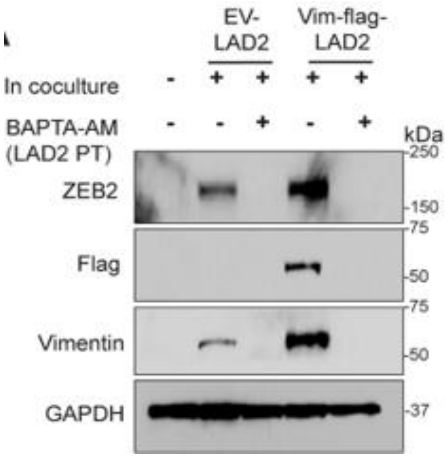

a)

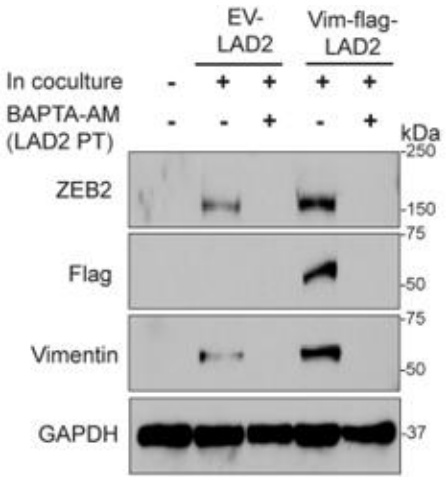

b)

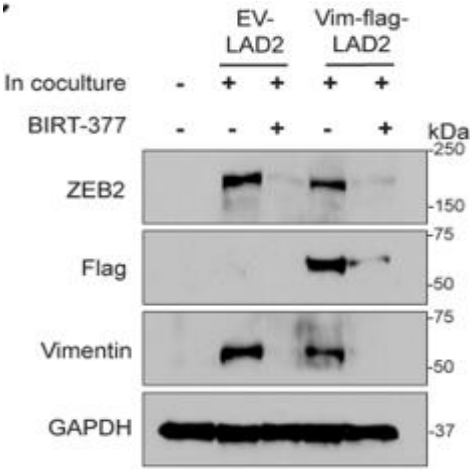

c)

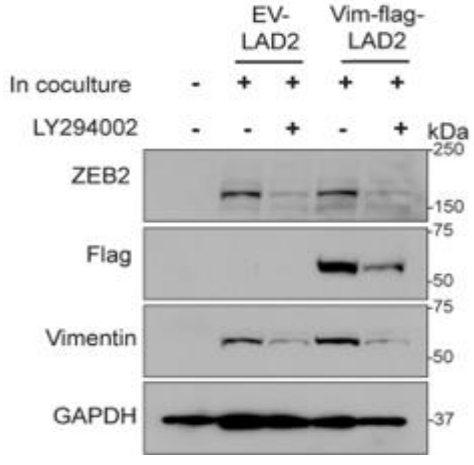

d)

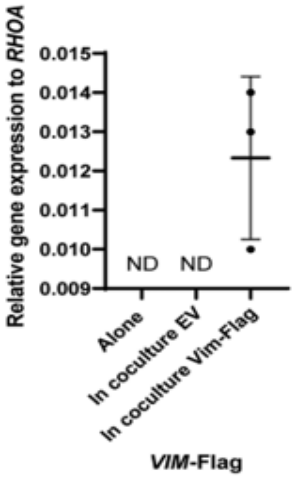

e)

Figure 7. Vimentin-Flag expressed in mast cells is directly conveyed to colorectal cancer cells. Panel a displays immunoblot analysis of HT-29 cells grown alone or cocultured with untreated empty-vector (EV) LAD2 cells, BAPTA-AM-pretreated (20 µM for 1 hour) EV LAD2 cells, untreated Vimentin-Flag-expressing (Vim-Flag) LAD2 cells, or BAPTA-AM-pretreated Vim-Flag LAD2 cells (N = 2). Panel b shows corresponding immunoblots for SW403 cells under the same coculture conditions (N = 1). Panel c presents immunoblots of HT-29 cells alone, cocultured with untreated EV LAD2 cells or EV LAD2 cells exposed to BIRT-377 (20 µM), untreated Vim-Flag LAD2 cells, or Vim-Flag LAD2 cells treated with BIRT-377 (20 µM) (N = 1). Panel d depicts immunoblots of HT-29 cells alone, cocultured with untreated EV LAD2 cells, EV LAD2 cells under LY294002 (50 µM), untreated Vim-Flag LAD2 cells, or Vim-Flag LAD2 cells under

LY294002 (50 μM) (N = 1). Panel e reports qRT-PCR quantification of Vim-Flag transcripts in HT-29 cells alone, cocultured with EV LAD2 cells, or cocultured with Vim-Flag-expressing LAD2 cells; ND denotes not detected. Data are shown as mean ± SD, with individual points indicating biological replicates.

The present investigation reveals that mast cells accumulate preferentially in BRAF-mutant colorectal cancers, probably due to chemoattractants secreted by tumor-associated secretory lineages. Upon arrival in the tumor bed, mast cells appear to facilitate epithelial-to-mesenchymal transition in cancer cells via a process requiring direct physical contact, intracellular calcium fluxes, and integrin engagement. A striking outcome of these close interactions is the intercellular delivery of cellular components from mast cells into tumor cells, exemplified by the conveyance of both Vimentin-Flag protein and its corresponding mRNA. This translocation mirrors the regulation of EMT marker induction, occurring through calcium-dependent and integrin-dependent pathways. These insights into the cancer-promoting functions of mast cells in BRAF-mutant colorectal tumors could highlight novel interventional strategies for managing these challenging malignancies.

The influence of mast cells on tumor biology is debated, as their effects depend on whether they reside at the tumor periphery or infiltrate deeply [38], and on cues from the surrounding milieu that dictate their activation state [29]. Consequently, mast cell contributions to patient outcomes may diverge across colorectal cancer subtypes, which differ in cellular composition and stromal features. Given established crosstalk between mast cells and secretory elements in healthy colonic tissue [8–12], we posited that the abundance of secretory phenotypes in BRAF-mutant tumors [7] drives mast cell infiltration. Ablation of secretory compartments in tumor lines indeed impaired mast cell chemotaxis in culture models, supporting the notion that tumor-derived secretory cells orchestrate mast cell recruitment, at least under experimental conditions. Accordingly, intratumoral mast cell presence may predominate in colorectal cancers characterized by prominent secretory differentiation.

Although mast cells have been linked to enhanced tumor progression, vascularization, and mesenchymal shifts in various contexts [13, 29, 31, 32], prior reports on their impact in colorectal cancer yield inconsistent conclusions. For instance, mast cell-derived conditioned medium has induced proliferative arrest and cell death in colorectal lines [16], yet bidirectional signaling between mast cells and tumor cells has also fostered expansion [15]. Traditionally, mast cell actions are attributed to discharged soluble cargo [29, 38]. Here, however, transferring conditioned medium—including potential exosomal contents—failed to elicit EMT marker changes in recipient cancer cells. Rather, live imaging and functional assays uncovered obligatory physical proximity, encompassing cell-cell adhesion and protrusive extensions from mast cells. Such intimate engagement proved essential for triggering mesenchymal alterations in tumor cells. This requirement for proximity may reconcile discrepancies across studies. To our knowledge, this represents the initial description of mast cell pro-tumorigenic activity in colorectal cancer executed through direct contact. Physical encounters between embedded mast cells and neoplastic epithelium could thus fuel tumor expansion and metastatic dissemination.

Transcriptomic profiling identified pronounced activation of the “integrin binding” module in mast cells following tumor cell exposure. Our results point to LFA-1/ICAM-1 pairing as a probable conduit for mast cell-tumor adhesion, akin to mast cell synapses with fellow immune effectors [39, 40]. Notably, pharmacological disruption of LFA-1 only partially curtailed EMT marker elevation, hinting at contributions from additional adhesion systems. Deeper elucidation of mast cell-integrin interfaces with colorectal tumor cells may uncover fresh targets for therapeutic intervention [41].

Using a calcium chelator, we demonstrated that mast cells (MCs) actively contribute to the promotion of the epithelial-mesenchymal transition (EMT) in colorectal cancer (CRC). Nevertheless, MCs retained the ability to physically interact with CRC cells even after calcium chelation, indicating that mere contact is insufficient to drive EMT in these cells. Calcium signaling in MCs regulates cytokine secretion, exocytosis, and the activation of various signaling pathways [26, 27]. Chelating calcium in MCs decreased AKT activation, but further studies are necessary to determine whether this reduction also affects other MC functions, such as exocytosis, which could influence EMT marker expression in CRC cells.

Various types of biological materials can be transferred between cells through contact-dependent mechanisms [34– 37]. Interestingly, we detected MC-derived Vim-

Flag mRNA within cocultured CRC cells, suggesting that MCs can directly deliver mRNA to cancer cells. It remains unclear whether the Vim-Flag protein observed in CRC cells originates directly from MCs or is synthesized in CRC cells from the transferred mRNA. In addition to transferring MC-encoded molecules, coculture with MCs also induced the expression of CRC cell–encoded EMT markers, as shown by activation of the HT-29 cell–encoded VIM-promoter mCherry reporter. We therefore propose that the direct transfer of VIM mRNA from MCs may establish a positive feedback loop that further enhances VIM expression from the endogenous promoter in CRC cells. Similarly, transfer of EMT-associated transcription factor ZEB2 could trigger endogenous Vimentin expression in CRC cells, given ZEB2's ability to bind the VIM promoter and induce transcription. However, the precise mechanisms of molecule transfer between MCs and CRC cells, as well as how these molecules stimulate EMT marker expression, require additional investigation. Notably, not all mCherry-positive cancer cells were observed in direct contact with MCs during imaging; this could be due to MCs detaching from some cancer cells during the four-hour coculture prior to imaging. Future work should clarify the duration of MC-cancer cell contact needed to induce EMT marker expression.

Whether MCs promote EMT marker expression in tumor epithelial cells through direct contact in vivo remains unknown. Furthermore, our study focused exclusively on MC–CRC interactions, but alterations in either cell type may also influence other cells in the tumor microenvironment. For instance, the chemokine CCL2 recruits and activates myeloid-derived suppressor cells in CRC and other cancers [42, 43]. We observed increased CCL2 expression in CRC cells cocultured with MCs, suggesting that MC–CRC contact may modify the cytokine milieu and consequently alter immune cell populations within the tumor. Further in vivo studies are needed to explore MC–CRC interactions and their potential impact on the tumor immune microenvironment.

Conclusion

This study has additional limitations, including the lack of data on the microsatellite instability (MSI) status of patient samples used in **Figure 1**. Given that MSI-positive CRCs show higher immune cell infiltration, MSI status could affect the results. Moreover, the absence of commercially available tissue microarrays annotated for BRAF mutation limited our ability to expand the tryptase immunohistochemistry (IHC) dataset. Increasing sample size with better annotation would strengthen the observed association between BRAF mutation and MC infiltration in primary CRC patient samples.

Acknowledgments: None

Conflict of Interest: None

Financial Support: None

Ethics Statement: None

References

1. Luo C, Cen S, Ding G, Wu W. Mucinous colorectal adenocarcinoma: clinical pathology and treatment options. Cancer Commun. 2019;39:13.
2. Biller LH, Schrag D. Diagnosis and treatment of metastatic colorectal cancer. JAMA. 2021;325:669.
3. Margonis GA, Buettner S, Andreatos N, Kim Y, Wagner D, Sasaki K, et al. Association of BRAF mutations with survival and recurrence in surgically treated patients with metastatic colorectal liver cancer. JAMA Surg. 2018;153:e180996.
4. Yaeger R, Cercek A, Chou JF, Sylvester BE, Kemeny NE, Hechtman JF, et al. BRAF mutation predicts for poor outcomes after metastasectomy in patients with metastatic colorectal cancer. Cancer. 2014;120:2316–24.
5. Motta R, Cabezas-Camarero S, Torres-Mattos C, Riquelme A, Calle A, Figueroa A, et al. Immunotherapy in microsatellite instability metastatic colorectal cancer: current status and future perspectives. J Clin Transl Res. 2021;7:511–22.
6. DeStefano Shields CE, White JR, Chung L, Wenzel A, Hicks JL, Tam AJ, et al. Bacterial-driven inflammation and mutant BRAF expression combine to promote murine colon tumorigenesis that is sensitive to immune checkpoint therapy. Cancer Discov. 2021;11:1792–807.
7. Miller SA, Policastro RA, Sriramkumar S, Lai T, Huntington TD, Ladaika CA, et al. LSD1 and aberrant DNA methylation mediate persistence of enteroendocrine progenitors that support BRAF-

mutant colorectal cancer. Cancer Res. 2021;81:3791–805.
8. Ahn MH, Kang CM, Park CS, Park SJ, Rhim T, Yoon PO, et al. Titanium dioxide particle - induced goblet cell hyperplasia: association with mast cells and IL-13. Respir Res. 200;6:34.
9. Grundemar L, Hakanson R. Neuropeptide Y, peptide YY and C-terminal fragments release histamine from rat peritoneal mast cells. Br J Pharmacol. 1991;104:776–8.
10. McGuckin MA, Hasnain SZ. Goblet cells as mucosal sentinels for immunity. Mucosal Immunol. 2017;10:1118–21.
11. Pelaseyed T, Bergström JH, Gustafsson JK, Ermund A, Birchenough GMH, Schütte A, et al. The mucus and mucins of the goblet cells and enterocytes provide the first defense line of the gastrointestinal tract and interact with the immune system. Immunol Rev. 2014;260:8–20.
12. Worthington JJ, Reimann F, Gribble FM. Enteroendocrine cells-sensory sentinels of the intestinal environment and orchestrators of mucosal immunity. Mucosal Immunol. 2018;11:3–20.
13. Visciano C, Liotti F, Prevete N, Cali' G, Franco R, Collina F, et al. Mast cells induce epithelial-to-mesenchymal transition and stem cell features in human thyroid cancer cells through an IL-8-Akt-Slug pathway. Oncogene. 2015;34:5175–86.
14. Ribatti D, Tamma R, Annese T. Epithelial-mesenchymal transition in cancer: a historical overview. Transl Oncol. 2020;13:100773.
15. Yu Y, Blokhuis B, Derks Y, Kumari S, Garssen J, Redegeld F. Human mast cells promote colon cancer growth via bidirectional crosstalk: studies in 2D and 3D coculture models. Oncoimmunology. 2018;7:e1504729.
16. Song F, Zhang Y, Chen Q, Bi D, Yang M, Lu L, et al. Mast cells inhibit colorectal cancer development by inducing ER stress through secreting Cystatin C. Oncogene. 2023;42:209–23.
17. Kirshenbaum AS, Yin Y, Bruce Sundstrom J, Bandara G, Metcalfe DD. Description and characterization of a novel human mast cell line for scientific study. Int J Mol Sci. 2019;20:5520.
18. Kirshenbaum AS, Akin C, Wu Y, Rottem M, Goff JP, Beaven MA, et al. Characterization of novel stem cell factor responsive human mast cell lines LAD 1 and 2 established from a patient with mast cell sarcoma/leukemia; activation following aggregation of FcεRI or FcγRI. Leuk Res. 2003;27:677–82.
19. Ladaika CA, Ghobashi AH, Boulton WC, Miller SA, O'Hagan HM. LSD1 and CoREST2 potentiate STAT3 activity to promote enteroendocrine cell differentiation in mucinous colorectal cancer. Cancer Res. 2025;85:52–68.
20. Newman AM, Liu CL, Green MR, Gentles AJ, Feng W, Xu Y, et al. Robust enumeration of cell subsets from tissue expression profiles. Nat Methods. 2015;12:453–7.
21. The Cancer Genome Atlas Network. Comprehensive molecular characterization of human colon and rectal cancer. Nature. 2012;487:330–7.
22. Schonhoff SE, Giel-Moloney M, Leiter AB. Neurogenin 3-expressing progenitor cells in the gastrointestinal tract differentiate into both endocrine and non-endocrine cell types. Dev Biol. 2004;270:443–54.
23. Li HJ, Ray SK, Kucukural A, Gradwohl G, Leiter AB. Reduced Neurog3 gene dosage shifts enteroendocrine progenitor towards goblet cell lineage in the mouse intestine. Cell Mol Gastroenterol Hepatol. 2021;11:433–48.
24. Huang B, Lei Z, Zhang GM, Li D, Song C, Li B, et al. SCF-mediated mast cell infiltration and activation exacerbate the inflammation and immunosuppression in tumor microenvironment. Blood. 2008;112:1269–79.
25. Zhu QC, Gao RY, Wu W, Qin HL. Epithelial-mesenchymal transition and its role in the pathogenesis of colorectal cancer. Asian Pacific J Cancer Prevent. 2013;14:2689–98.
26. Suzuki Y, Inoue T, Ra C. Calcium signaling in mast cells: focusing on L-type calcium channels. Adv Exp Med Biol. 2012:740:955–77.
27. Ma HT, Beaven MA. Regulators of Ca2+ signaling in mast cells: potential targets for treatment of mast cell-related diseases? Adv Exp Med Biol. 2011;716:62–90.
28. Tsai M, Grimbaldeston M, Galli SJ. Mast cells and immunoregulation/immunomodulation. Adv Exp Med Biol. 2011;716:186–211.
29. Varricchi G, Galdiero MR, Loffredo S, Marone G, Iannone R, Marone G, et al. Are mast cells MASTers in cancer? Front Immunol. 2017;8:424.
30. Komi DEA, Redegeld FA. Role of mast cells in shaping the tumor microenvironment. Clin Rev Allergy Immunol. 2020;58313–25.

31. Ribatti D, Crivellato E. Mast cells, angiogenesis, and tumour growth. Biochim Biophys Acta Mol Basis Dis. 2012;1822:2–8.
32. Elieh Ali Komi D, Wöhrl S, Bielory L. Mast cell biology at molecular level: a comprehensive review. Clin Rev Allergy Immunol. 2020;58:342–65.
33. Lightsey S, Sharma B. Natural killer cell mechanosensing in solid tumors. Bioengineering. 2024;11:328.
34. Dupont M, Souriant S, Lugo-Villarino G, Maridonneau-Parini I, Vérollet C. Tunneling nanotubes: intimate communication between myeloid cells. Front Immunol. 2018;9:43.
35. Mattes B, Scholpp S. Emerging role of contact-mediated cell communication in tissue development and diseases. Histochem Cell Biol. 2018;150:431–42.
36. Eugenin E, Camporesi E, Peracchia C. Direct cell-cell communication via membrane pores, gap junction channels, and tunneling nanotubes: medical relevance of mitochondrial exchange. Int J Mol Sci. 2022;23:6133.
37. Yoneyama Y, Zhang RR, Kimura M, Cai Y, Adam M, Parameswaran S, et al. Inter-cellular mRNA transfer alters human pluripotent stem cell state. Proc Natl Acad Sci USA. 2025;122:e2413351122.
38. Liu X, Li X, Wei H, Liu Y, Li N. Mast cells in colorectal cancer tumour progression, angiogenesis, and lymphangiogenesis. Front Immunol. 2023;14:1209056.
39. Carroll-Portillo A, Cannon JL, te Riet J, Holmes A, Kawakami Y, Kawakami T, et al. Mast cells and dendritic cells form synapses that facilitate antigen transfer for T cell activation. J Cell Biol. 2015;210:851–64.
40. Stelekati E, Bahri R, D'Orlando O, Orinska Z, Mittrücker HW, Langenhaun R, et al. Mast cell-mediated antigen presentation regulates CD8+ T cell effector functions. Immunity. 2009;31:665–76.
41. Slack RJ, Macdonald SJF, Roper JA, Jenkins RG, Hatley RJD. Emerging therapeutic opportunities for integrin inhibitors. Nat Rev Drug Discov. 2022;21:60–78.
42. Kumar V, Patel S, Tcyganov E, Gabrilovich DI. The nature of myeloid-derived suppressor cells in the tumor microenvironment. Trends Immunol. 2016;37:208–20.
43. Chun E, Lavoie S, Michaud M, Gallini CA, Kim J, Soucy G, et al. CCL2 promotes colorectal carcinogenesis by enhancing polymorphonuclear myeloid-derived suppressor cell population and function. Cell Rep. 2015;12:244–57.